

## Research Article

# Remediation of Azure A Dye from Aqueous Solution by Using Surface-Modified Coal Fly Ash Extracted Ferrospheres by Mineral Acids and Toxicity Assessment

Virendra Kumar Yadav <sup>1,2</sup>, Gajendra Kumar Inwati <sup>3</sup>, Daoud Ali,<sup>4</sup> G. Gnanamoorthy <sup>5</sup>,  
Sweta Parimita Bera,<sup>1</sup> Samreen Heena Khan,<sup>2</sup> Nisha Choudhary,<sup>6</sup> Gokhlesh Kumar,<sup>7</sup>  
Tejula Prasad Chaurasia,<sup>8</sup> and Anup Basnet <sup>9</sup>

<sup>1</sup>Department of Microbiology, School of Sciences, P P Savani University, Surat, 394125 Gujarat, India

<sup>2</sup>Research and Development Centre, YNC ENVIS Pvt. Ltd, New Delhi 110059, India

<sup>3</sup>Department of Chemistry, HVHP Institute of Post Graduate Studies and Research, Sarva Vishwavidyalaya, Kadi, 382715 Gujarat, India

<sup>4</sup>Department of Zoology, College of Science, King Saud University, PO Box 2455, Riyadh 11451, Saudi Arabia

<sup>5</sup>Department of Inorganic Chemistry University of Madras, Chennai, Tamil Nadu, 600025, India

<sup>6</sup>Department of Environment Sciences, School of Sciences, P P Savani University, Surat, 394125 Gujarat, India

<sup>7</sup>Clinical Division of Fish Medicine, University of Veterinary Medicine Vienna, 1210 Vienna, Austria

<sup>8</sup>School of Allied Health Sciences, Jaipur National University, Jaipur, Rajasthan 302017, India

<sup>9</sup>Department of Microbiology, Saint Xaviers College, Maitighar, Kathmandu, 44600, Nepal

Correspondence should be addressed to Anup Basnet; [basnet.a@sxc.edu.np](mailto:basnet.a@sxc.edu.np)

Received 24 November 2021; Revised 31 December 2021; Accepted 18 January 2022; Published 30 January 2022

Academic Editor: Lakshmiopathy R

Copyright © 2022 Virendra Kumar Yadav et al. This is an open access article distributed under the Creative Commons Attribution License, which permits unrestricted use, distribution, and reproduction in any medium, provided the original work is properly cited.

The Indian coal fly ash (CFA) is composed of 5-15% ferrous fractions. The variation in percentage depends on the source of coal and the operating conditions of the thermal power plants. The present research work reports the recovery of ferrous particles from CFA by the wet magnetic separation method. The morphological, elemental, and chemical properties of the extracted ferrous fractions were analyzed. In order to achieve surface-modified ferrospheres, the extracted ferrospheres were treated with concentrated HCl followed by sonication. The instrumental analysis reported the ferrous composition is around 16% by weight and belongs to class F. The toxicity of CFA was determined on normal human lung (BEAS-2B) cells using MTS assay. The results showed that CFA's induced cell toxicity in a dose-dependent manner. The ferrous particles were spherically shaped with various sizes ranging from 200 nm to 7000 nm. It was crystalline in nature and is a mixture of hematite and magnetite. The particles were found to be associated with alumina, silica, oxygen, and traces of Ca, Mg, Ti, and C. The surface-modified ferrospheres were used for the remediation of Azure A dye by batch adsorption study. The removal percentage of dye was 25.03%, within 30 minutes at neutral pH, i.e., 7.2. The surface-modified ferrospheres show potential as an alternate, more economical, and reusable adsorbent for the remediation of Azure A dye in the industries or in common effluent treatment plants. Moreover, the recovery of surface-modified ferrospheres using an external magnet and the reuse of the particles make the material much economical for dye removal at an industrial scale.

## 1. Introduction

Nano-adsorbents have paved their way in our everyday lives. They are used in medicines, environmental remediation,

electronics, manufacturing of different commodities, and many more such applications. Although quite effective, their usage is a bit expensive affair. The synthesizing of nanoparticles is a costly process. To withstand this issue, a lot of

alternative synthesizing techniques are being designed all over the globe. One such method is the use of coal fly ash (CFA). For remediating the pollutants from wastewater, this can be used either directly or along with their components [1, 2]. CFA has several naturally structured materials like cenospheres [3, 4], ferrospheres [5], and carbon materials [6]. These are widely used as an adsorbent for the remediation of both organic as well as inorganic pollutants from wastewater [7, 8]. Coal contain silica, alumina, and iron, so their ashes are generally composed of the oxides of alumina and silica along with a certain percentage of Fe, Ca, Ti, and Mg [9]. The composition of CFA is determined by the nature of the coal source, operating parameters, and design of thermal power plants (TPPs) [10]. CFA has both crystalline and amorphous phases [11], where the crystalline forms quartz, magnetite, mullite [12], and hematite in a matrix of aluminosilicate glass [13, 14]. Fe is the third largest element found in the CFA followed by Al and Si [15]. These elements are present in the oxide phases like magnetite, hematite, maghemite, and goethite as reported by various scientists [16]. CFA have ferrous content in the range of 5-15% based on the type of coal used in the thermal power plants (TPPs) [17, 18]. When coal is burned, pyrite is converted to hematite at 400-700°C and to maghemite if it is further heated up to 1390°C [19]. The crystallinity and composition of ferrous particles depend on the melting point and thermal conditions of microparticle formation [20]. The ferrous particles extracted from CFA find applications in ferrous-dependent industries [21], steel-based industries, coke-smelting industries [22], fillers [23], petroleum cracking [24], catalysis for profound oxidation [25], oxidative coupling of CH<sub>4</sub> (OCM) [26], thermolysis of petroleum residue, adsorbents for environmental clean-up [27], and wastewater treatment [17].

The dry and wet slurry separation methods are the two basic types of ferrous extraction methods for CFA [17]. In dry form, ferrous is separated by conveyor belts where one end has a strong magnet. The wet slurry separation technique involves mixing CFA with water and then recovering the ferrous particles by using a strong magnet [16]. Sharonova et al. and Shoumkova extracted the ferrous fractions and revealed their shape and elemental composition from Russian TPPs [28, 29]. The former group recovered eight types of ferrospheres (FS) whose sizes were in the range of 0.4 to 0.02 mm by the dry method. The latter group recovered FS having impurities of elements like Al, Si, S, and Ca. Xue and Lu [30] revealed the microstructures of FS in CFA isolated by magnetic separation technique and reported the presence of magnetite and hematite phases of Fe in FS [31]. The recovered FS were reported to have Al, Si, S, and Ca. Their shape was smooth, polygonal, dendritic, and granular and had molten drop characteristics [32]. Oliveira et al. recovered spinel magnetite from the silico-aluminous CFA from TPPs of the France region and analyzed them by sophisticated instruments [33]. Shoumkova recovered FS from Russian TPP and exhibited that Al, Mg, and Ti were the dominant elements in the FS [29]. Azure A dye is one of the major dye effluents from the textile industry [34]. The high concentration in the effluent further contaminates

the rivers and other water bodies, thereby affecting the flora and fauna of the surrounding area. Moreover, this dye is remediated in nature at a very low rate [35]. Here, investigators have carried out surface modification of FS by mineral acid like conc. HCl and conc. sulphuric acid. This was then applied for the remediation of Azure A dye from the aqueous solutions [8]. The major advantage of using mineral acid surface-modified FS as an adsorbent is that it will make the dye adsorption process economical due to the utilization of the waste material. The adsorbent is magnetic in nature, so the adsorbent can be easily manipulated externally using a magnetic field [36]. It can also be recycled and easily recovered after the completion of the adsorption experiment. From all the reported works, it was found that CFA-extracted FS always have Ca, Al, Si, Ca, Mg, Na, O, P, etc., in them [37, 38].

The main objective of the present research work is to extract and characterize the ferrous particles from CFA. The particles were then further analyzed for their purity and morphology by the wet slurry separation method. The extracted FS were surface-functionalized by treating with mineral acids (sulphuric acid and hydrochloric acid) by ultrasonication technique along with heating. The surface-functionalized FS and extracted FS were analyzed by sophisticated instruments for their detailed information. Further, the potential of surface-functionalized FS was assessed for the removal of Azure A dye from the aqueous solution by batch adsorption study.

## 2. Materials and Method

**2.1. Chemical and Reagents.** The MTS assay kit (ab 197010) was procured from abcam (Cambridge, CB2 0AX, UK), Dulbecco's modified Eagle's medium (DMEM), antibiotics, and fetal bovine serum (FBS) were procured from Gibco (USA), coal fly ash and neodymium magnet (circular shape) (4 cm W × 0.5 cm H) were procured from A2Z magnet New Delhi (India), glass beakers (250 ml), Milli-Q water, Petri plate, and ethanol were procured from Schenzen (China), and Conc. HCl and Conc. H<sub>2</sub>SO<sub>4</sub> used were by RENKEM.

**2.2. Sampling Area.** The CFA was collected in the autoclaved plastic silos directly from the electrostatic precipitators of TPPs, Kota, Rajasthan, India. The sample was then oven-dried at 105°C prior to analysis.

**2.3. Magnetic Extraction of Ferrous Particles from CFA.** The XRF analysis of CFA revealed that the CFA sample had more than 15% ferrous fractions by weight. This is much greater than the normal levels found in Indian CFA's. The ferrous-rich silico-aluminous CFA was concentrated with ferrous particles, by an external magnet. A slurry of CFA was prepared by adding 10 grams of CFA in 100 ml of Milli-Q water. The ferrous fractions were extracted from the slurry using an external magnet. Again, 10 grams of CFA was added into the slurry, and ferrous fractions were recovered with the magnet. This step was repeated numerous times until a considerable amount of ferrous fractions were recovered. The ferrous fractions were washed with

Milli-Q water, and a neodymium magnet was placed at the bottom of the beaker to minimize the loss of ferrous fractions during washing. The washing step was repeated until sufficient purity was obtained. Further, the obtained ferrous fractions were washed with ethanol in order to remove any organic content present in the ferrous fractions. Finally, the obtained ferrous fractions (shown in Figure 1) were oven-dried at 50°C till complete dryness occurred, and all the moisture was removed. Finally, the dried ferrous fractions were stored in a vial and characterized by the analytical instruments for detailed information like purity, elemental composition, and morphology.

**2.4. Acidic Treatment of Extracted Ferrospheres.** FS obtained from the CFA was treated with different concentrated mineral acids, i.e., conc. sulphuric acid and hydrochloric acid. A mixture of FS and mineral acids was taken separately in a 100 ml round bottom flask. The solid to liquid ratio was about 1:10. Further, both mixtures were placed inside an ultrasonicator device (Sonar 40 kHz). The mixture was heated at 65-70°C, for one hour. Once the reaction was complete, the mixture was cooled to room temperature (RT), followed by centrifugation at 7000 rpm for 10 minutes. This was followed by the decantation of the supernatant while retaining the residue. The residue was washed 2-3 times with Milli-Q water to eliminate the acidic moieties present on the surface of the residues. Finally, the obtained residue was oven-dried at 50°C prior to instrumental analysis.

**2.5. Preparation of 0.1 mg Solution of Azure A Dye Solution.** About 1 mg Azure A dye was taken in 100 ml Milli-Q water and stirred for a few minutes in order to dissolve the particles. Further, the mixture was filtered using a Whatman filter paper no. 42 and stored in a glass bottle. For the remediation of the dye from the solution, about 80 ml of dye was taken in a beaker to which 0.1 mg of FS was added. The stirring was carried out on a magnetic stirrer at 500 rpm for one hour at room temperature. An aliquot was taken after every 10 minutes and analyzed by the UV-Vis for the detection of the concentration of Azure A dye in the aqueous solution.

**2.6. Characterization of Ferrospheres.** The FT-IR analysis was done to detect the functional group present in the FS by preparing a solid pellet by mixing KBr and sample in the ratio of 198 mg and 2 mg, respectively. The FT-IR analysis was done in the infrared IR region of 400-4000  $\text{cm}^{-1}$  at a resolution of 2  $\text{cm}^{-1}$  by using PerkinElmer-made instrument, model no. SP-65. Raman spectroscopy was done by placing the ferrous particles on a glass coverslip with a laser intensity of 625 nm and 750 nm. The spectra were obtained by passing a beam of light through the samples thrice. The analysis was carried out by using Witec alpha+, Germany-made instrument, in the region of 200-4000  $\text{cm}^{-1}$ . The XRD was done for the phase identification in the FS, where the XRD patterns ( $2\theta$  of 20-70°) were recorded by using the D-8 Advance, Bruker (Germany), equipped with an X'celerator. The step size was 0.02 and a time of 5 seconds per step at 40 kV voltage and a current of 30 mA. The morphological analysis of the FS was done by all three microscopic tech-



FIGURE 1: Ferrous fractions extracted from CFA.

niques, i.e., FESEM, TEM, and atomic force microscopy (AFM). FS and surface modified FS were analyzed by the FESEM Nova, NANOSEM 450 (FEI, Netherlands) from two different places. For analysis, dry powder samples were spread on the carbon tape which in turn was placed on the aluminum stub. The sample was coated with gold sputtering, before analysis. The elemental analysis of the samples was done by an Oxford-made EDS analyzer attached with the FESEM. The focusing of the beam on a specific spot of ferrous particles was done at variable magnifications and at 20 kV. For TEM analysis, a drop of the sample was dispersed on a carbon-coated copper grid from the dispersed sample which was later oven-dried prior to sample analysis. The morphological and elemental analysis was done by using FEI Model Tecnai G2 20 Twin (200 kV) (USA) instruments operated at a voltage of 200 kV. The AFM of the sample was done by dispersing the ferrous particles in Milli-Q water as prepared in the above step for HR-TEM analysis. The dispersed sample was cast on a clean glass slide, i.e., 2-3 drops, and the sample was allowed to dry in an oven at 50°C for 4-5 hours. The slide was then washed with Milli-Q water to remove loosely attached particles and dried in an oven at 45°C above conditions, before analysis. The measurement to obtain the 2D and 3D images of the ferrous particles was done by Park System-made instrument, model: XE-70. The physical property measurement system (PPMS) was done for the magnetic measurements of the ferrous sample by using model no. PPMS 300 k, i.e., at RT with the magnetic field from -7000 k to +7000 k. About 0.3 g ferrous particles were taken and wrapped in paraffin tape. Further, the sample was placed inside the quartz-made probe (tube) for the analysis.

**2.7. Cell Culture and Exposure of CFA.** The toxicity tests were studied on BEAS-2B (normal human lung) cell (CAT NO. 95102433) (Sigma-Aldrich Chemie GmbH, USA). The cells were subcultured in DMEM with 10 percent FBS and  $1 \times 10^4$   $\mu\text{g/ml}$  antibiotics at a 5%  $\text{CO}_2$  incubator at 37°C. Cells at 75% confluence were subcultured into 96-well plate



cytotoxicity experiments. BEAS-2B cells were grown overnight before exposure to CFA. The stock solution of CFA was prepared in double-distilled water (DDW) at the rate of 1 mg/ml DDW. It was further diluted as per the experimental dosage (0–10  $\mu\text{g}/\text{ml}$ ). Control cells were not exposed to CFA and were considered as controls.

**2.8. MTS Assay.** MTS assay was performed as per kit (ab 197010) manufacturer's instructions. The MTS test is based on the reduction of the MTS tetrazolium compound by live BEAS-2B cells to produce a colored formazan salt that is soluble in DMEM. The absorbance was determined at 495 nm using a BioTek Epoch plate reader (BioTek Instruments, Winooski, VT, USA) and Gen5 software (version 1.09).

**2.9. Statistical Analysis.** The statistical analyses were performed using SPSS 26.0 software (IBM). Differences were analyzed using a one-way ANOVA test. Values of  $*p < 0.05$  were considered statistically significant.

### 3. Results and Discussion

**3.1. Morphological Analysis of Ferrospheres by FESEM.** The morphological features of CFA-extracted ferrous particles were studied using FESEM. In Figures 2(a) and 2(b) FESEM, the micrograph shows that the ferrous particles (FPs) are spherical in shape and sizes 0.2–7.8  $\mu\text{m}$ . The presence of non-ferrous particles was also observed. The ferrous particles are spherical in shape and have a comparatively higher amount of Fe than the aluminosilicate spheres; hence, it is called FS [39]. Based on the surface texture, two types of FS have an either smooth or rough surface as shown in Figures 2(b) and 2(d). The particles in Figure 2(b) are smooth in texture while all others have a rough texture. The rough surface FS [40] have either angular-shaped particles or spherule depositions [41]. These ferrous-rich concentrates on the surface of FS provide magnetic properties [42]. While in smooth FS, the ferrous particles are distributed evenly and have very little Fe content [43]. Figure 2(c) reveals that the FS have spherule deposition on their surface. Besides this, there are a few non-FS which have rectangular depositions on their surface. Figure 2(d) shows FS with angular particle depositions and minute spherule depositions. The molten drop-like structure [37] is generally the molten liquid of the intrinsic Fe-bearing phases in the coal. There are few elliptical-shaped FS which might have acquired the shape due to the improper formation of particles during cooling of CFA and its minerals in the TPPs [44]. Figures 3(a)–3(d) show the single FS at higher resolution, where the rough-surfaced FS surface has angular and polygonal depositions. A typical structure of a rare “*crystal-line structure*” [45] is seen present as a rectangular pattern on the surface in Figure 3(a), while Figure 3(b) also shows FS with an angular deposition on their surface. Figure 3(c) shows FESEM micrographs of FS having different types of ferrous particle depositions on their surface. Few FS have spherule deposits, while few have angular ferrous particle depositions, which are responsible for providing FS with a rough surface texture. Several investigators have also

reported the presence of rough-surfaced structures of ferrous particles in fly ash from various parts of the globe [46], while Figure 4(d) shows FS with minute spherule deposits on their surface.

The size of the individual FS varies from 400 to 700 nm in Figures 3(a)–3(d). In Figures 3(a)–3(d), the rough-surfaced FS indicates the depositions of angular or spherule-shaped particles on the preformed aluminosilicate spheres in the thermal power plants [47]. Such particles which are deposited are iron oxides that provide magnetic properties to the rough-surfaced particles. These iron oxides are deposited on the surface of the preformed matrix of Al-Si during cooling and condensation of the particle.

The proper spherical shape of FS implies that the particulates have formed at high-temperature combustion via a series of nucleation, coagulation, and condensation of vaporized material methods [48]. Similar results were also reported by Silva et al. who obtained crystalline FS in size range of 10 to 100  $\mu\text{m}$ , which have mainly hematite, ferrous sulphate, and Fe-aluminum silicate glass using EDS [49, 50]. The external and internal structures of FS depend on the various parameters like furnace design, the chemical composition of coal combusted, formation temperature, or cooling procedures [51]. Even though FS have different sizes and surface textures, structurally, they have a mainly rough or smooth surface where the rough is an either polygonal or granulated type [44].

**3.2. Electron Diffraction Spectroscopy (EDS) for Elemental Analysis.** Figure 4 reveals the EDS analysis of the CFA-extracted FS, where the EDS spot exhibits Fe content (44%), which is quite high and confirms the area of magnetic crystals, i.e., magnetic phases. O was followed by Fe in the FS which was about (38%), which indicates iron oxide phases in the FS. Besides this, EDS spectra of FS also have Si (6.4%), Al (5.5%), C (1.3%), and Ca (1.1%) and traces of Mg, P, Ti, and Na which sum up about 1.92%. The reason for the association of trace elements is due to the deposition of elements during coalescence and cooling of molten CFA. The obtained FESEM micrographs and EDS spectra are in support to the work done by Xue and Lu [30]. In these silico-aluminous-rich iron oxides, aluminosilicate glass acts as a matrix on which Fe and Ca are embedded on them. Iron oxides present in the CFA are generally called as “*spinel*” which are formed when the concentration of iron is more in molten matrix [4, 30].

**3.3. Morphological Analysis by TEM.** TEM is used as an efficient technique for studying the microstructure, morphology, and surface texture of a particle. Figures 5(a) and 5(b) show both spherical as well as rod-shaped particles, whose sizes vary from 600 nm to 1200 nm. The size of spherical particles varies from 300 nm to 900 nm. The spherical-shaped particles are dark black in color, which indicates the electron-rich elements like Fe and indicates FS, while the rod-shaped particles are light black in color, which indicates the aggregation of carbon particles, soots, and other particles to give a rod-shape appearance [6].

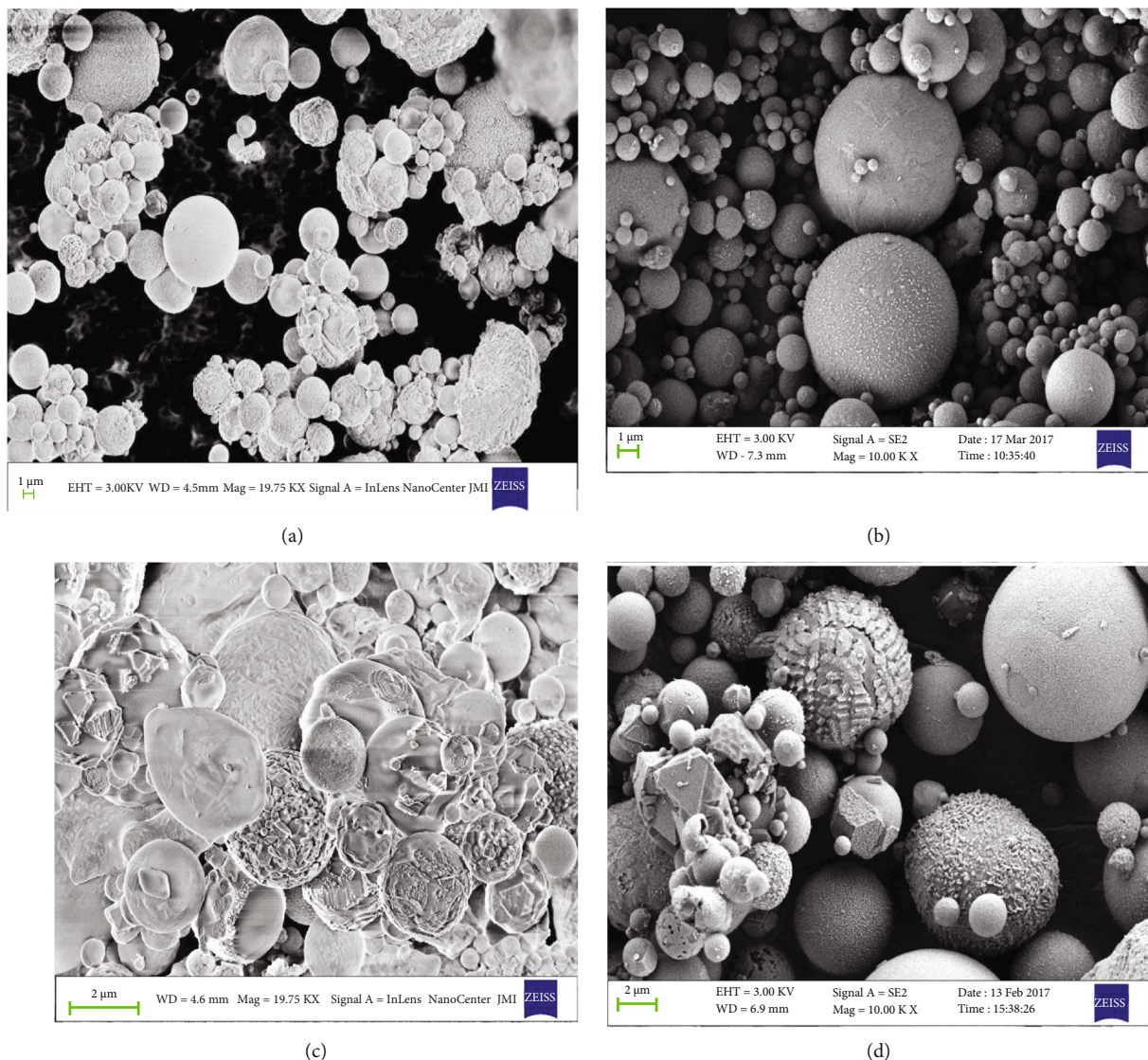


FIGURE 2: FESEM micrographs of CFA ferrospheres (a–d).

Figure 5(c) shows TEM micrographs of FS and aluminosilicate spheres of sizes 200 nm to 1200 nm which are aggregated together. The particles are dark black in color, which indicate the ferrous particles. Figure 5(d) shows a single FS particle of size up to 2 microns, which is dark black in color. Figure 5(e) shows lattice fringes or d-spacing of the FS particles, while Figure 6(f) exhibits the scattering area electron diffraction (SAED) pattern of FS.

From the SAED pattern, it is clearly visible that the FS are polycrystalline in nature, which indicates a well crystalline pattern of ferrous on FS. The polycrystalline nature of ferrous particles of CFA was reported earlier by Bhatt et al. [10]. The EDS spectra in Figures 6(a) and 6(b) reveal the presence of various elements in the FS. In Figure 6(a), EDS spectra show peaks for Fe and O along with traces of Si, Al, and Ca which clearly indicates the ferrous-rich spheres. Fe is present in the highest amount by weight percentage in Figure 6(a), followed by O, Si, Ca, and Al, which is 68.46%, 28.11%, 0.39%, and 0.12%, respectively. While

Figure 6(b) reveals EDS spectra of less Fe-rich FS, in Figure 6(b), the spectra of EDS display O, Al, Si, and Ca found to be richer, i.e., 58.42%, 5.36%, 20.63%, and 9.26% than the presence of ferrous particles, which is 6.34%.

**3.4. Atomic Force Microscopy Analysis for 3D Structure of Ferrospheres.** AFM is commonly used for analyzing the direct height, volume, and 3D structure of the FS particles. Both 2D and 3D images of FS were obtained by adjusting the scan rate, scan size, and set point parameters of AFM imaging.

The FS topography is exhibited in Figure 7(a) and is a 2D image, while a 3D image is shown in Figure 7(b). The spherical shape and crystalline nature of FS obtained by AFM were in accordance with the FESEM and TEM micrographs. The IOPs, mullite [12], and quartz provide the crystalline nature to the FS, while glassy quartz form is responsible for amorphous nature. The irregularity in shape, on the surface topography of the FS, shows the randomness



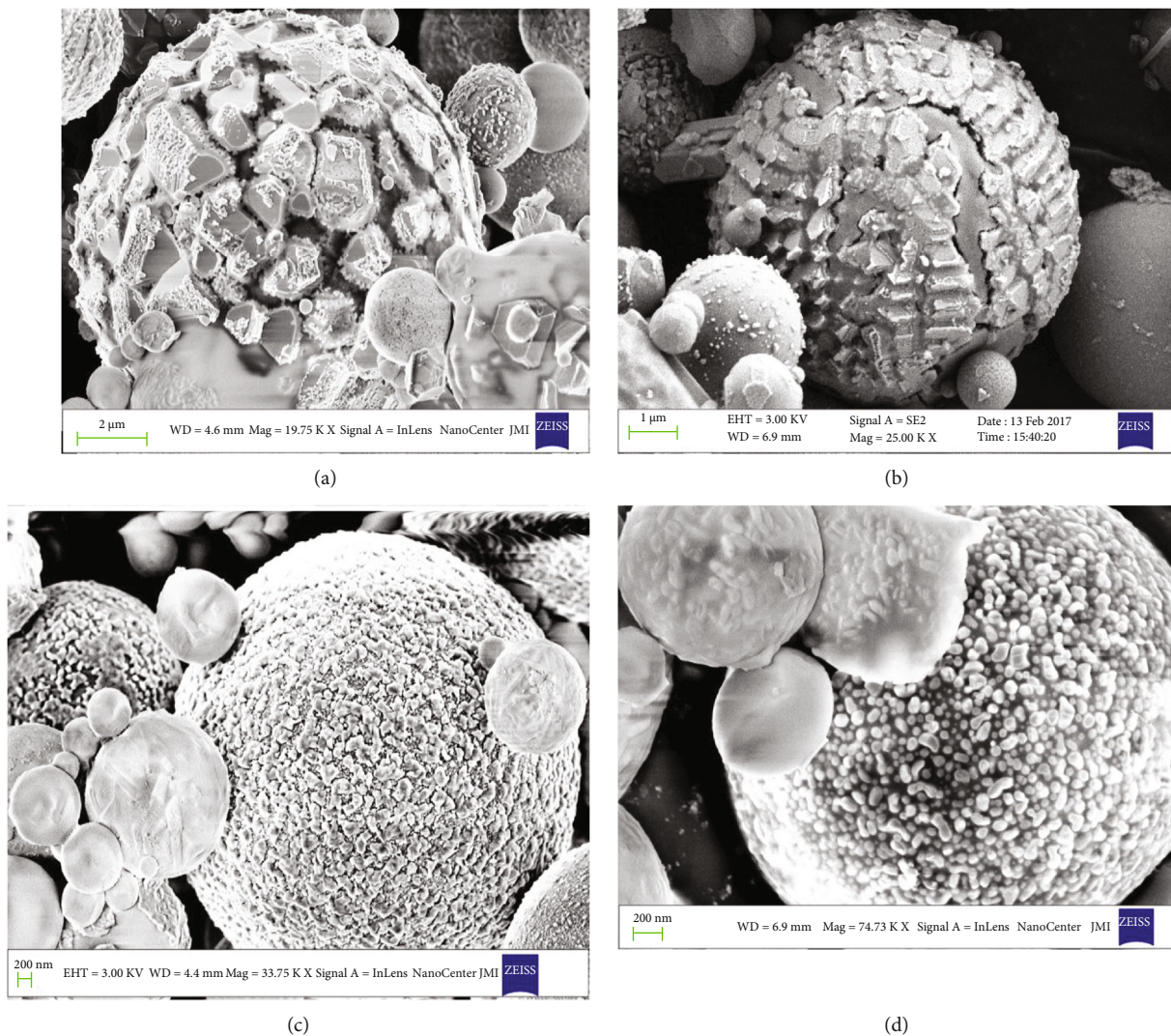


FIGURE 3: FESEM micrographs of FS: (a) angular deposits, (b) crystalline pattern, (c) spherules deposits, and (d) minute spherule deposits.

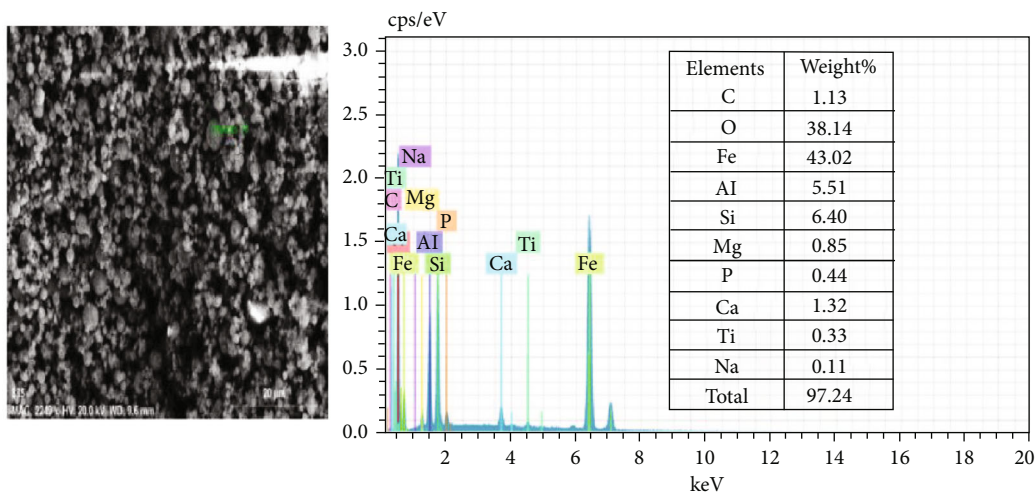


FIGURE 4: EDS spot, EDS spectra, and elemental composition of ferrospheres.

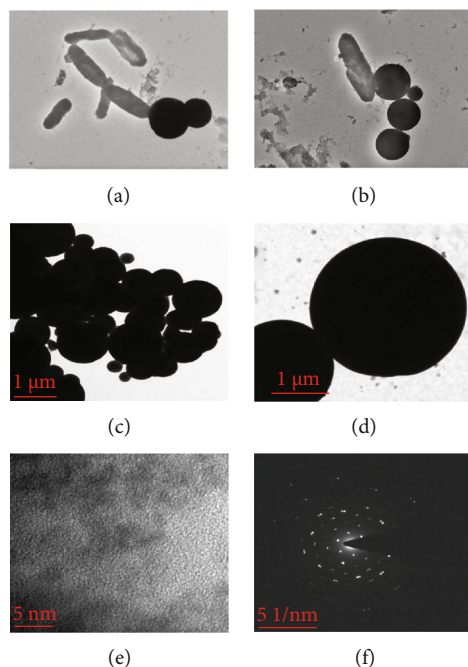


FIGURE 5: TEM micrographs of (a–d) CFA FS, (e) d-spacing, (f) and SAED pattern.

of FS. The topographical image of the particles shows the surface of the particles which is also coordinated with TEM characterization.

**3.5. FT-IR and Raman Spectroscopy.** The FTIR spectra of the FS in Figure 8(a) reveal three characteristic bands around  $1082\text{ cm}^{-1}$  which is due to Si-O-Si glass,  $576\text{ cm}^{-1}$  Fe-O stretching vibrations of bond, and the band at  $474\text{ cm}^{-1}$  is due to the symmetric bending vibrations of Fe-O or due to Si-O-Al bond [52, 53].

The peak for Si is due to the presence of silica as an impurity in the FS due to its abundance in the CFA. The silicate peak is due to the associated silica along with the FS. The peak at  $576\text{ cm}^{-1}$  is due to Fe-O stretching vibrations, and the peak at  $474\text{ cm}^{-1}$  is due to the symmetric bending vibrations of Fe-O and could be due to Si-O-Al [54]. Since there is a presence of quartz and mullite in the FS as impurities, the peaks of Si-O-Al and Si-O-Si are quite obvious [55]. The impurities in the form of quartz and mullite were also supported by the EDS and XRD data. Another important technique used for the identification of ferrous-rich particles is Raman spectroscopy which also reveals the functional groups. A typical Raman spectrum of a CFA FS is shown in Figure 8(b). Raman spectra confirm the presence of hematite in the FS as it has peaks at  $295\text{ cm}^{-1}$  which are due to the Fe-O stretching by hematite, while the peaks at  $408\text{ cm}^{-1}$  are due to the Fe-O stretching by hematite in the FS. The peaks at  $628\text{ cm}^{-1}$  imply the presence of magnetite [56]. Raman confirms the presence of mixtures of iron oxides (magnetite, maghemite, and hematite) in the FS.

**3.6. X-Ray Diffraction for Phase Identification.** Figure 9(a) shows the typical XRD diffractogram of CFA-extracted FS. From the various literature studies of class F CFA, it was

found that the major minerals present in CFA are quartz [57], mullite, and iron oxide [55]. The XRD peaks at  $33.8^\circ$  and  $35.6^\circ$  indicate iron oxides [58], hematite, and magnetite, respectively [59]. The major peak at  $33.8^\circ$  is due to hematite, while peaks at  $35.6^\circ$  and  $54.3^\circ$  are due to magnetite, which are very sharp peaks and indicate that the FS are crystalline in nature [59].

The peaks at  $24.2^\circ$  and  $30.1^\circ$  are due to the quartz and mullite, respectively [60], which are present in trace amount with the FS. The presence of Al, Si as quartz, and mullite was also justified by the TEM, FESEM-EDS, and FTIR analysis. CFA particles are generally complex mixtures of silica, alumina, and iron along with calcium, Mg, and  $\text{TiO}_2$ . Therefore, the recovered FS are associated with a certain amount of traces of these elements. Magnetization of the CFA-isolated FS was performed at RT and hysteresis loop, and the magnetization of the FS was obtained. In Figure 9(b), magnetization ( $M_s$ ) of magnetic particles is shown with respect to the function of applied magnetic field ( $H$ ) per time. The effect of applied magnetic field on the saturation magnetization is studied in the range of  $-7000$  to  $+7000$ . The magnetization ( $M_s$ ) value of FS is  $0.31\text{ emu}$ . This could be due to the good homogeneity, higher degree of crystallization, and uniform morphology of the particles. The retentivity ( $M_r$ ) of the particle is  $58.14\text{ emu}$ , while the coercivity ( $H_{ci}$ ) is  $182.67\text{ G}$ .

### 3.7. Effect of Conc. HCl and $\text{H}_2\text{SO}_4$ Treatment on the Ferrospheres

**3.7.1. Hydrochloric Acid Treated Ferrospheres.** The effect of concentrated HCl and sulphuric acid on the FS was observed on the basis of FESEM images. In the case of HCl-treated ferrosphere residues, one can observe the large-sized pores

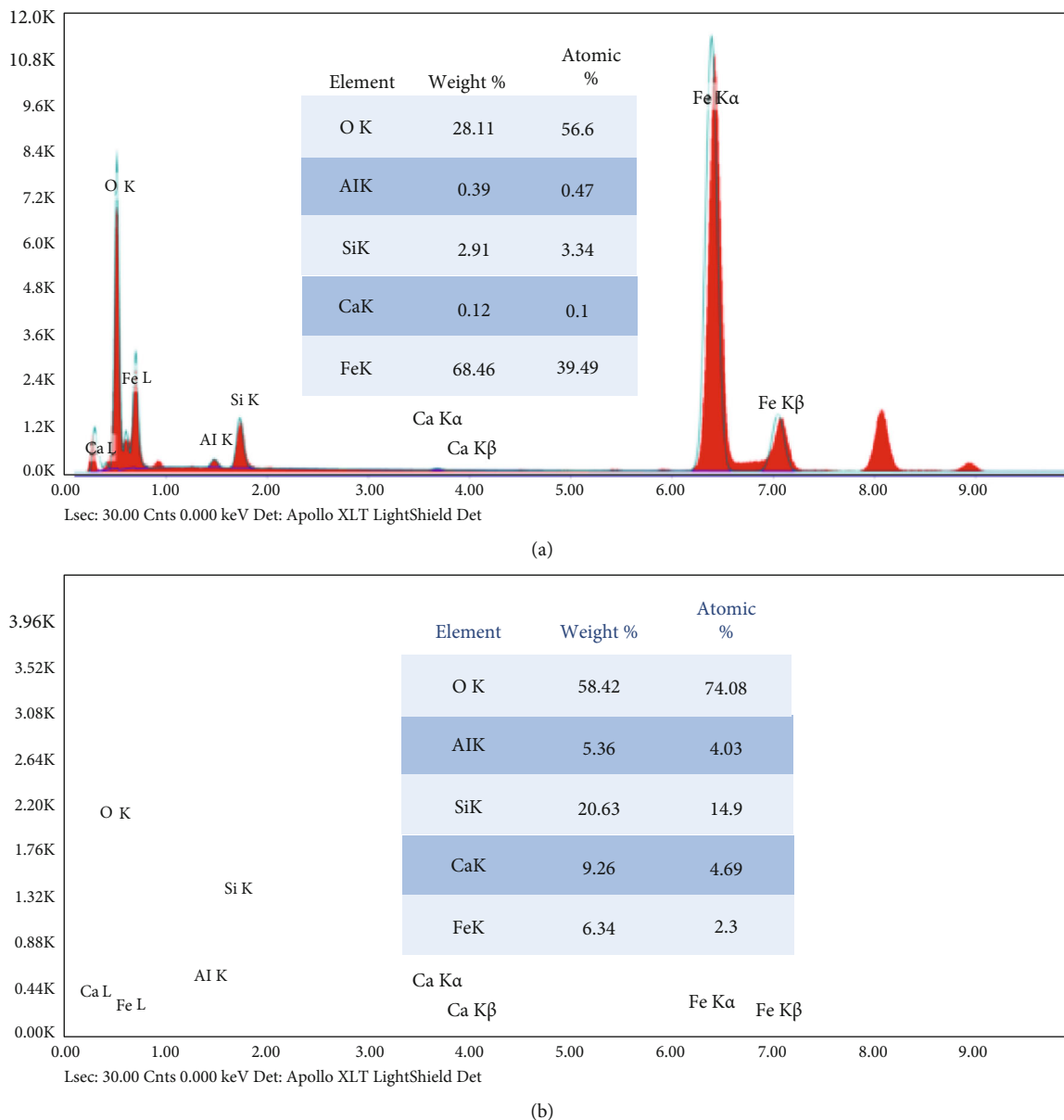


FIGURE 6: EDS spectra and elemental analysis of FS: (a) high ferrous-rich and (b) less ferrous-rich particles.

on FS. HCl acts as a strong leaching agent that causes thorough leaching of the ferrous. Conc. HCl is a strong leaching agent and acts vigorously on the FS resulting in the appearance of large-sized pores on the surface as seen in Figures 10(a), 10(c), and 10(d). It is also valuable to note that leaching efficiency increases with the increase in conc. of HCl as the temperature rises.

**3.7.2. Sulphuric Acid Treated Ferrosphere Residue.** The leached residue obtained from the leaching process ( $H_2SO_4$ ) was examined for surface morphology by FESEM. As it is evident from Figures 11(a)–11(d), sulphuric acid acts as a weak leaching agent as compared to hydrochloric acid. The smaller pores appear on the FS due to the less leaching of ferrous. Figure 11(c) shows smaller-sized pores on the FS. Thus, the leaching agent plays important roles in determin-

ing the surface morphology as the stronger the leaching agent, the larger the surface pores.

**3.8. Batch Adsorption Study of Azure Dye by Surface-Modified Ferrospheres.** The percent dye decolorization and adsorption capacity of surface-modified FS were calculated using the following equation:

$$\% \text{Decolorization} = \frac{A_0 - A_t}{A_0} \times 100, \quad (1)$$

$$q_t (\text{mg/g}) = \frac{(A_0 - A_t)V}{M}, \quad (2)$$

where  $A_0$  = initial Azure A dye concentration ( $\text{mg l}^{-1}$ ),  $A_t$  = concentration of Azure A dye at a particular time ( $\text{mg l}^{-1}$ )



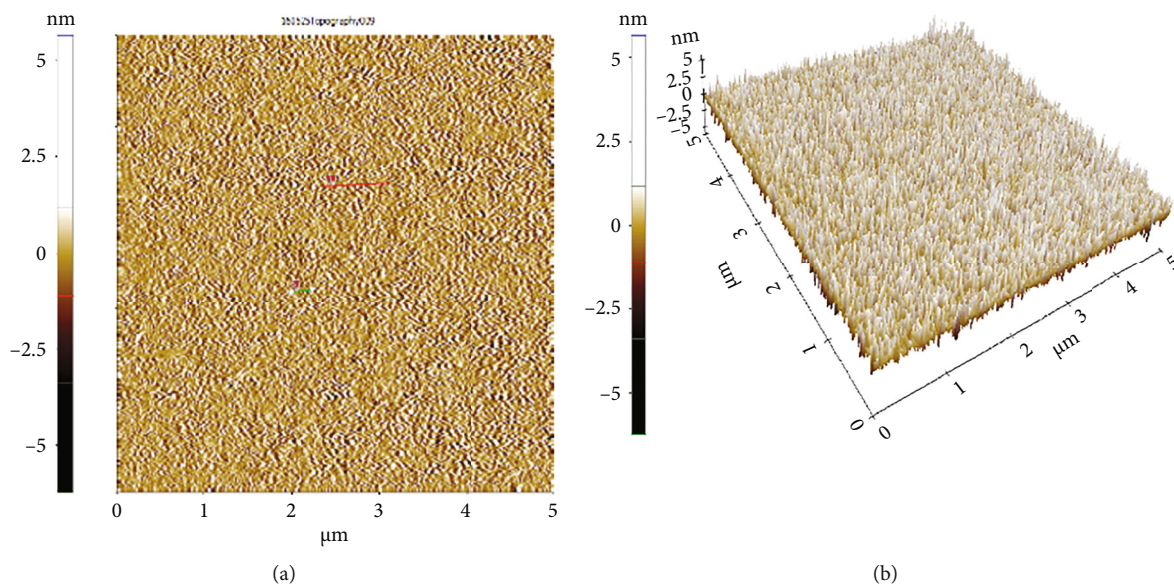


FIGURE 7: AFM images of CFA ferrospheres: (a) 2D and (b) 3D.

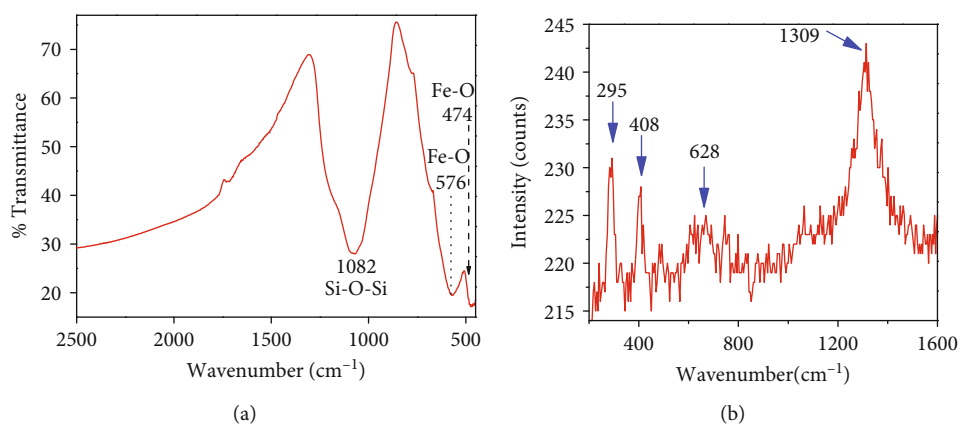


FIGURE 8: (a) FTIR spectra and (b) Raman spectra of CFA ferrospheres.

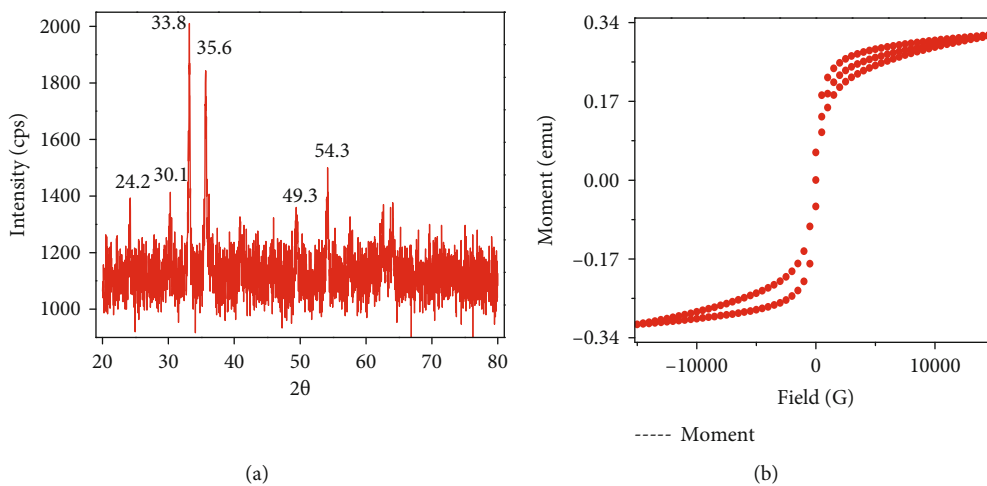


FIGURE 9: (a) XRD diffractograms of ferrospheres and (b) magnetic strength of ferrospheres by PPMS.

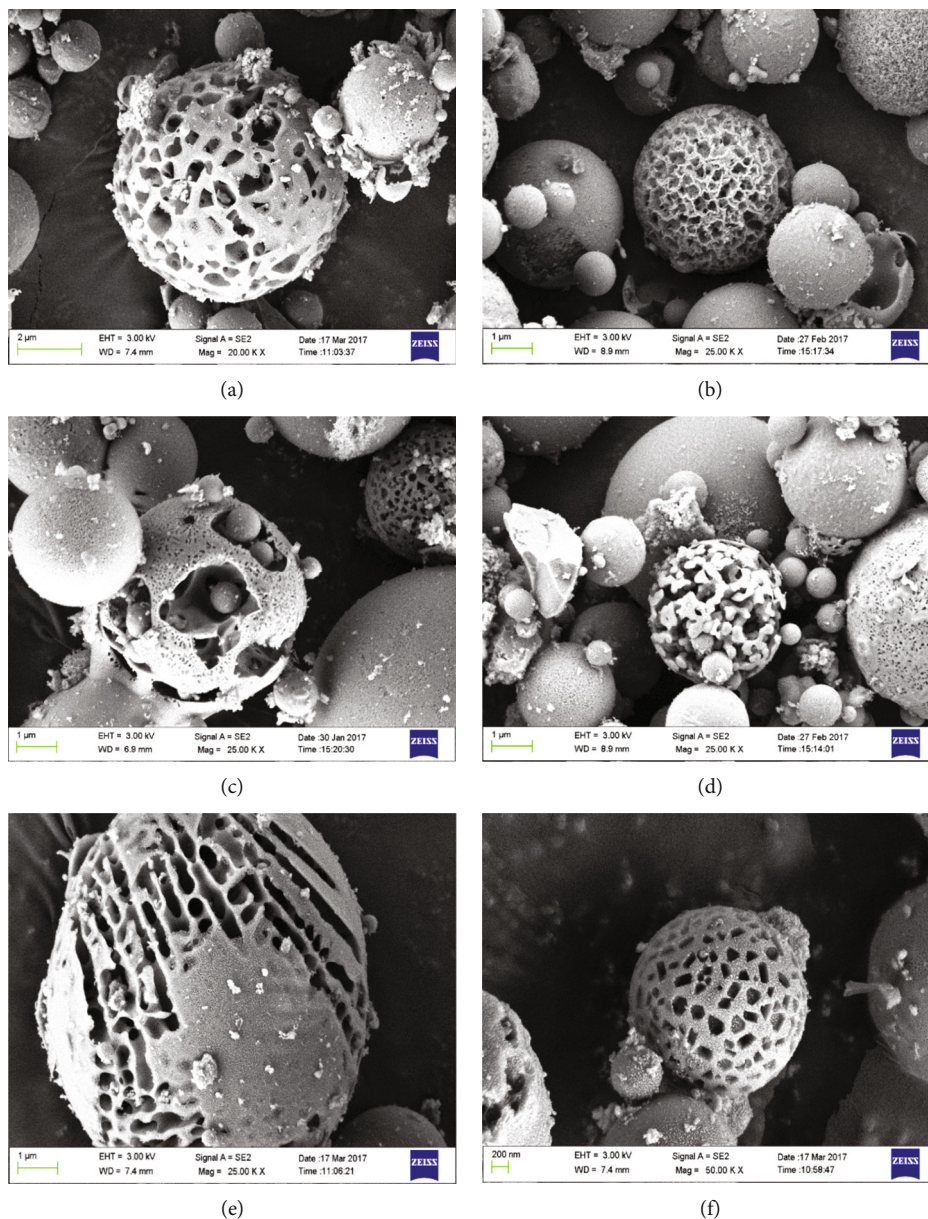


FIGURE 10: FESEM images (a–f) of conc. HCl-treated ferrospheres.

$V$  = volume of solution (liter), and  $M$  = mass of surface – modified ferrospheres (gm).

The concentration of Azure A dye continuously decreased from 0 minutes to 30 minutes as shown in Figure 12, while the dye removal percentage gradually increased from 0 to 10 minutes. At 15 minutes, the percentage removal of Azure A dye decreased; but after that, the percentage removal of Azure A dye increased drastically. It reached maximum removal at 30 minutes which was 25.03%, while the lowest removal percentage was observed at 15 minutes which was just 1.76%, while the percentage removal of Azure A dye at 5, 10, and 25 minutes was 2.96%, 4.2%, and 15.34% as shown in Figure 13.

Several investigators also used CFA as a low-cost adsorbent for the removal of dyes from wastewater. Mohan et al.

removed crystal violet and basic fuchsin by using CFA [61]. Wang et al. reported the remediation of various dyes from wastewater by using modified CFA particles. The investigators tried to remediate methylene blue, crystal violet, and rhodamine B which were basic dyes by using HCl-treated CFA. They also treated the CFA with microwave irradiation and found that conc. HCl-treated CFA showed better adsorption capacity for the basic dyes from wastewater [62]. Here, the approach was almost similar, but instead of using direct CFA particles, investigators used CFA-extracted conc. HCl-treated ferrous particles. Out of both approaches, our approach was more significant as the ferrous particles could be easily manipulated by using an external magnet and also it could be used several times for the remediation of dyes which is not possible with the CFA



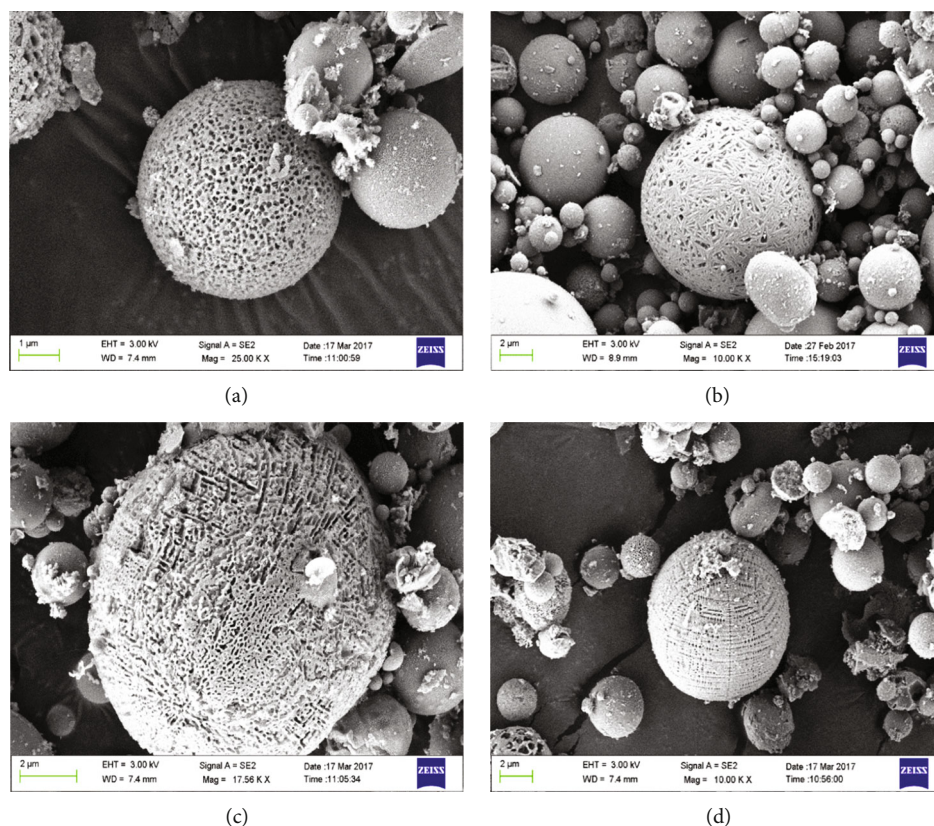


FIGURE 11: FESEM images (a–f) of conc. H<sub>2</sub>SO<sub>4</sub>-treated FS.

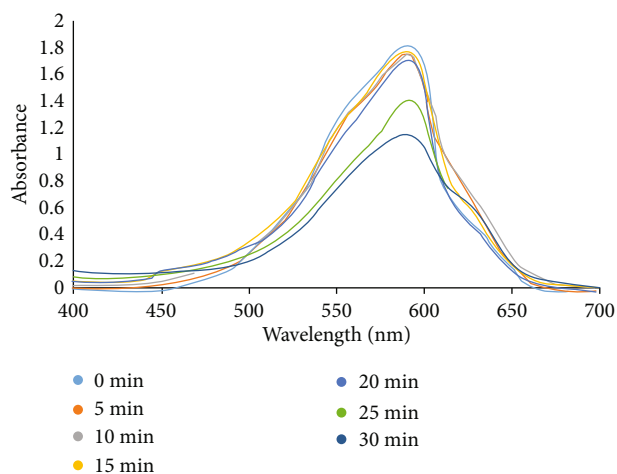


FIGURE 12: Absorption spectrum representing time-dependent removal of Azure A dye by surface-modified ferrospheres.

particles. So, in the use of surface-modified FS, the removal of the dye makes the remediation process very economical as the source material for FS, i.e., CFA is available and free of cost [63].

**3.9. Effect of pH on the Adsorption of CR Dye from the Solution.** Often, the charge on adsorbents and their degree of ionization in the solution are influenced by the pH, because hydrogen and hydroxyl ions are actively adsorbed

on the surface of the catalysts or adsorbents. As a result, the pH moieties such as H<sup>+</sup> and OH<sup>-</sup> influence the adsorption of other ions released from the dye molecules. The adsorptive operation is affected by changes in pH due to the separation of functional groups on the active open sites of the adsorbent. Therefore, the reaction kinetics and equilibrium constraints of the adsorption rate affect. The presence of H<sup>+</sup> ions on the surface means the more acidic media (solution) favor the adsorption of anions at lower pH, whereas the excess of OH<sup>-</sup> groups (basic environment) on the surface of the catalyst favors the adsorption of cations at higher pH. In our case, an excess of surface sites possesses as the adsorption experiments was conducted with modified ferrous particles (higher active open surfaces), resulting in a larger active site under the used pH range (pH = 7.2 distilled water) to regulate the adsorption character on catalyst surfaces. Probably, the used aqueous solution (pH = 7.2) facilitates an optimized pH condition to adsorb CR dye molecules as it has both the cationic and anionic moieties which may actively interact with catalyst surfaces [64].

Earlier, Nguyen et al. used hydrothermally synthesized Mg-Al-layered double hydroxide (Al LDH) for the remediation of CR dye from the aqueous solutions at different pH (2.0, 4.0, 6.0, 8.0, 10.0, and 12.0). The investigators found that pH affects the charges on the surface of adsorbent and the degree of dissociation of the anionic dye. It was concluded that pH drastically alters the surface charge of Mg-Al LDH, ultimately the removal of dye. Lower pH, i.e., (2.0 and 4.0), is acidic in nature and may dissolve the CR dye



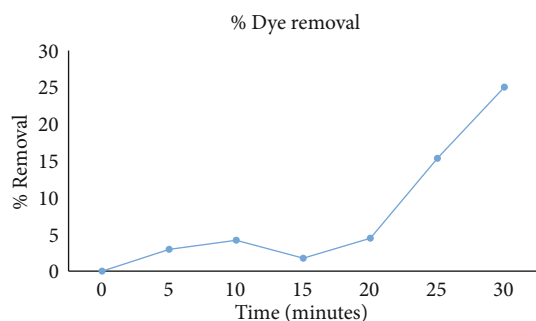


FIGURE 13: Percentage removal of Azure A dye by surface-modified ferrospheres.

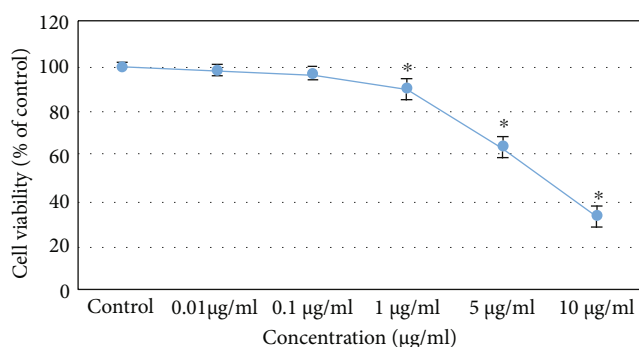


FIGURE 14: Cytotoxicity of CFA on BEAS-2B cells for 24 h. Each value represents the average  $\pm$  SE of the three experiments  $n = 3$  \* $p < 0.5$  versus control.

molecule from the medium, so an optimum result was obtained near neutrality, i.e., 6.0 in this case. This could be explained to the chemical form of dye in the aqueous solution and various functional groups present on the surface of the adsorbent at a particular pH [65].

**3.10. Cytotoxicity.** The toxicity of CFA was measured by MTS assay. The cell viability result was represented in Figure 14. Toxicity of CFA on BEAS-2B cells in a dose-dependent manner and maximum toxicity was observed at 10  $\mu\text{g/ml}$  CFA (Figure 14). Toxicity of CFA (0.01, 0.1, 1.0, 5.0, and 10  $\mu\text{g/ml}$ ) was observed 1.6%, 3%, 10%, 36%, and 67% for 24 h on BEAS-2B cell line, respectively (Figure 14).

## 4. Conclusions

The CFA has 15% ferrous particles which could act as a sustainable and economical source of ferrous particles as well as an adsorbent. The extracted ferrous particles from CFA waste were spherical in shape, and their size varies from 200 nm to 2 microns. The ferrospheres have magnetic properties due to the deposition of Fe in the form of oxides during the melting and cooling of the molten slag of coal. The iron oxides deposited on the ferrospheres were in mixed phases, i.e., magnetite, maghemite, and hematite as confirmed by the XRD and Raman spectroscopy. The iron oxide particles deposited on the surface of ferrospheres were crystalline in nature as confirmed by the XRD and TEM. The

ferrospheres have impurities in the form of Al, Si, and Ca. This makes it suitable for the removal of pollutants from the aqueous solution. The utilization of such waste, economical, and eco-friendly material makes the remediation process a low-cost adsorption technique. The Azure A dye removal percentage was about 25.03%, within 30 minutes. This indicates the use of surface-modified ferrospheres for dye removal as a potentially more economical alternative that can be used in the industries.

## Data Availability

The data sets used and analyzed during the current study are available within the article only.

## Conflicts of Interest

The authors declare that there is no conflict of interest.

## Authors' Contributions

VKY was responsible for the conceptualization. VKY, GKI, DA, GG, and AB were responsible for the methodology. VKY, AB, SPB, DA, SHK, NC, GK, and TPC wrote and corrected the manuscript.

## Acknowledgments

This work was funded by Researchers Supporting Project number (RSP-2021/165), King Saud University, Riyadh, Saudi Arabia.

## References

- [1] V. K. Yadav, K. K. Yadav, V. Tirth et al., "Extraction of value-added minerals from various agricultural, industrial and domestic wastes," *Materials*, vol. 14, no. 21, p. 6333, 2021.
- [2] Y. Virendra Kumar and P. Priti Raj, "Fly ash properties and their applications as a soil ameliorant," in *Amelioration Technology for Soil Sustainability*, K. R. Ashok, Ed., pp. 59–89, IGI Global, Hershey, PA, USA, 2019.
- [3] J. Wrona, W. Żukowski, D. Bradło, and P. Czupryński, "Recovery of cenospheres and fine fraction from coal fly ash by a novel dry separation method," *Energies*, vol. 13, no. 14, p. 3576, 2020.
- [4] V. K. Yadav, K. K. Yadav, V. Tirth et al., "Recent advances in methods for recovery of cenospheres from fly ash and their emerging applications in ceramics, Composites, Polymers and Environmental Cleanup," *Crystals*, vol. 11, no. 9, p. 1067, 2021.
- [5] E. Strzałkowska, "Morphology, chemical and mineralogical composition of magnetic fraction of coal fly ash," *International Journal of Coal Geology*, vol. 240, article 103746, 2021.
- [6] J. Alam, V. K. Yadav, K. K. Yadav et al., "Recent advances in methods for the recovery of carbon nanominerals and poly-aromatic hydrocarbons from coal fly ash and their emerging applications," *Crystals*, vol. 11, no. 2, p. 88, 2021.
- [7] Y. Virendra Kumar, C. Nisha, K. Samreen Heena et al., "Synthesis and characterisation of nano-biosorbents and their applications for waste water treatment," in *Handbook of Research on Emerging Developments and Environmental*

- Impacts of Ecological Chemistry*, D. Gheorghe and V. Ashok, Eds., pp. 252–290, IGI Global, Hershey, PA, USA, 2020.
- [8] V. K. Yadav, N. Choudhary, D. Ali et al., “Experimental and computational approaches for the structural study of novel Ca-rich zeolites from incense stick ash and their application for wastewater treatment,” *Adsorption Science & Technology*, vol. 2021, article 6066906, pp. 1–12, 2021.
- [9] S. K. Behera, S. Chakraborty, and B. C. Meikap, “Deminerallization mechanism and influence of parameters on high ash Indian coal by chemical leaching of acid and alkali solution,” *International Journal of Coal Science & Technology*, vol. 5, pp. 142–155, 2018.
- [10] A. Bhatt, S. Priyadarshini, A. Acharath Mohanakrishnan, A. Abri, M. Sattler, and S. Techapaphawit, “Physical, chemical, and geotechnical properties of coal fly ash: a global review,” *Case Studies in Construction Materials*, vol. 11, article e00263, 2019.
- [11] K. Yan, Y. Guo, Z. Ma, Z. Zhao, and F. Cheng, “Quantitative analysis of crystalline and amorphous phases in pulverized coal fly ash based on the Rietveld method,” *Journal of Non-Crystalline Solids*, vol. 483, pp. 37–42, 2018.
- [12] V. K. Yadav, P. Saxena, C. Lal et al., “Synthesis and characterization of mullites from silicoaluminous fly ash waste,” *International Journal of Applied Nanotechnology Research*, vol. 5, no. 1, pp. 10–25, 2020.
- [13] P. Koshy, N. Ho, V. Zhong et al., “Fly ash utilisation in mullite fabrication: development of novel percolated mullite,” *Minerals*, vol. 11, no. 1, p. 84, 2021.
- [14] N. N. Anshits, M. A. Fedorchak, E. V. Fomenko, E. V. Mazur-ova, and A. G. Anshits, “Composition, structure, and formation routes of blocklike ferrospheres separated from coal and lignite fly ashes,” *Energy & Fuels*, vol. 34, pp. 3743–3754, 2020.
- [15] W. Franus, M. M. Wiatros-Motyka, and M. Wdowin, “Coal fly ash as a resource for rare earth elements,” *Environmental Science and Pollution Research*, vol. 22, pp. 9464–9474, 2015.
- [16] D. Valeev, I. Kunilova, A. Alpatov, A. Varnavskaya, and D. Ju, “Magnetite and carbon extraction from coal fly ash using magnetic separation and flotation methods,” *Minerals*, vol. 9, no. 5, p. 320, 2019.
- [17] V. K. Yadav and M. H. Fulekar, “Advances in methods for recovery of ferrous, alumina, and silica nanoparticles from fly ash waste,” *Ceramics*, vol. 3, pp. 384–420, 2020.
- [18] K. M. Zierold and C. Odoh, “A review on fly ash from coal-fired power plants: chemical composition, regulations, and health evidence,” *Reviews on Environmental Health*, vol. 35, pp. 401–418, 2020.
- [19] J. Yu, Y. Han, Y. Li, P. Gao, and W. Li, “Mechanism and kinetics of the reduction of hematite to magnetite with CO–CO<sub>2</sub> in a micro-fluidized bed,” *Minerals*, vol. 7, p. 209, 2017.
- [20] E. V. Fomenko, N. N. Anshits, L. A. Solovyov et al., “Magnetic fractions of PM<sub>2.5</sub>, PM<sub>2.5–10</sub>, and PM<sub>10</sub> from coal fly ash as environmental pollutants,” *ACS Omega*, vol. 6, no. 30, pp. 20076–20085, 2021.
- [21] H. Unterweger, R. Tietze, C. Janko et al., “Development and characterization of magnetic iron oxide nanoparticles with a cisplatin-bearing polymer coating for targeted drug delivery,” *International Journal of Nanomedicine*, vol. 9, pp. 3659–3676, 2014.
- [22] T. Ju, S. Han, Y. Meng, and J. Jiang, “High-end reclamation of coal fly ash focusing on elemental extraction and synthesis of porous materials,” *ACS Sustainable Chemistry & Engineering*, vol. 9, pp. 6894–6911, 2021.
- [23] D. Paul, M. Suresh, and M. Pal, “Utilization of fly ash and glass powder as fillers in steel slag asphalt mixtures,” *Case Studies in Construction Materials*, vol. 15, article e00672, 2021.
- [24] E. M. Opiso, C. B. Tabelin, C. V. Maestre, J. P. J. Aseniero, I. Park, and M. Villacorte-Tabelin, “Synthesis and characterization of coal fly ash and palm oil fuel ash modified artisanal and small-scale gold mine (ASGM) tailings based geopolymer using sugar mill lime sludge as Ca-based activator,” *Heliyon*, vol. 7, no. 4, article e06654, 2021.
- [25] Z. Lei, Q. Lingbo, S. Hao et al., “Formation of fly ash catalysts and selection of a matrix binder and its application in denitration,” *ACS Omega*, vol. 5, pp. 31567–31574, 2020.
- [26] S. N. Vereshchagin, E. V. Kondratenko, E. V. Rabchevskii, N. N. Anshits, L. A. Solov’ev, and A. G. Anshits, “New approach to the preparation of catalysts for the oxidative coupling of methane,” *Kinetics and Catalysis*, vol. 53, no. 4, pp. 449–455, 2012.
- [27] D. Sunjidmaa, G. Batdemberel, and S. Takibai, “A study of ferrospheres in the coal fly ash,” *Open Journal of Applied Sciences*, vol. 9, pp. 10–16, 2019.
- [28] O. M. Sharonova, N. N. Anshits, M. A. Fedorchak, A. M. Zhizhaev, and A. G. Anshits, “Characterization of ferrospheres recovered from high-calcium fly ash,” *Energy & Fuels*, vol. 29, pp. 5404–5414, 2015.
- [29] A. S. Shoumkova, “Magnetic separation of coal fly ash from Bulgarian power plants,” *Waste Management & Research*, vol. 29, pp. 1078–1089, 2011.
- [30] Q. Xue and S. Lu, “Microstructure of ferrospheres in fly ashes: SEM, EDX and ESEM analysis,” *Journal of Zhejiang University-SCIENCE A*, vol. 9, no. 11, pp. 1595–1600, 2008.
- [31] V. V. Zyryanov, S. A. Petrov, and A. A. Matvienko, “Characterization of spinel and magnetospheres of coal fly ashes collected in power plants in the former USSR,” *Fuel*, vol. 90, pp. 486–492, 2011.
- [32] A. Fernández-Jiménez, I. García-Lodeiro, O. Maltseva, and A. Palomo, “Mechanical-chemical activation of coal fly ashes: an effective way for recycling and make cementitious materials,” *Frontiers in Materials*, vol. 6, p. 51, 2019.
- [33] M. L. S. Oliveira, F. Marostega, S. R. Taffarel et al., “Nano-mineralogical investigation of coal and fly ashes from coal-based captive power plant (India): an introduction of occupational health hazards,” *Science of the Total Environment*, vol. 468–469, pp. 1128–1137, 2014.
- [34] T. Shindhal, P. Rakholiya, S. Varjani et al., “A critical review on advances in the practices and perspectives for the treatment of dye industry wastewater,” *Bioengineered*, vol. 12, pp. 70–87, 2021.
- [35] B. Lellis, C. Z. Fávaro-Polonio, J. A. Pamphile, and J. C. Polonio, “Effects of textile dyes on health and the environment and bioremediation potential of living organisms,” *Biotechnology Research and Innovation*, vol. 3, pp. 275–290, 2019.
- [36] O. V. Kharissova, H. V. R. Dias, and B. I. Kharisov, “Magnetic adsorbents based on micro- and nano-structured materials,” *RSC Advances*, vol. 5, pp. 6695–6719, 2015.
- [37] H. Liu, Q. Sun, B. Wang, P. Wang, and J. Zou, “Morphology and composition of microspheres in fly ash from the Luohuang power plant, Chongqing, Southwestern China,” *Minerals*, vol. 6, no. 2, p. 30, 2016.
- [38] S. Rajendran, G. K. Inwati, V. K. Yadav et al., “Enriched catalytic activity of TiO<sub>2</sub> nanoparticles supported by activated carbon for noxious pollutant elimination,” *Nanomaterials*, vol. 11, no. 11, p. 2808, 2021.

- [39] E. Strzałkowska, "Morphology and chemical composition of mineral matter present in fly ashes of bituminous coal and lignite," *International Journal of Environmental Science and Technology*, vol. 18, pp. 2533–2544, 2021.
- [40] N. N. Anshits, E. V. Fomenko, and A. G. Anshits, "Composition–structure relationship and routes of formation of block-like ferrospheres produced by pulverized combustion of two coal types," *ACS Omega*, vol. 6, no. 40, pp. 26004–26015, 2021.
- [41] J. Ma, D. Wang, S. Zhao, P. Duan, and S. Yang, "Influence of particle morphology of ground fly ash on the fluidity and strength of cement paste," *Materials*, vol. 14, no. 2, p. 283, 2021.
- [42] E. V. Sokol, V. M. Kalugin, E. N. Nigmatulina, N. I. Volkova, A. E. Frenkel, and N. V. Maksimova, "Ferrospheres from fly ashes of Chelyabinsk coals: chemical composition, morphology and formation conditions," *Fuel*, vol. 81, pp. 867–876, 2002.
- [43] X. Zhang, G. Wu, T. Yao, C. Zhang, and Y. Yue, "Characterization of individual fly ash particles in surface snow at Urumqi Glacier No. 1, Eastern Tianshan," *Chinese Science Bulletin*, vol. 56, no. 32, pp. 3464–3473, 2011.
- [44] Y. Zhao, J. Zhang, J. Sun, X. Bai, and C. Zheng, "Mineralogy, chemical composition, and microstructure of ferrospheres in fly ashes from coal combustion," *Energy & Fuels*, vol. 20, pp. 1490–1497, 2006.
- [45] K. L. Aughenbaugh, P. Stutzman, and M. C. G. Juenger, "Identifying glass compositions in fly ash," *Frontiers in Materials*, vol. 3, p. 1, 2016.
- [46] K. Mirković, N. Tošić, and G. Mladenović, "Effect of different types of fly ash on properties of asphalt mixtures," *Advances in Civil Engineering*, vol. 2019, Article ID 8107264, 11 pages, 2019.
- [47] B. Smieja-Król, B. Fiałkiewicz-Kozieł, A. Michalska, T. Krzykowski, and D. Smolka-Danielowska, "Deposition of mullite in peatlands of southern Poland: implications for recording large-scale industrial processes," *Environmental Pollution*, vol. 250, pp. 717–727, 2019.
- [48] H. Liu, Y. Wang, and J. O. L. Wendt, "Particle size distributions of fly ash arising from vaporized components of coal combustion: a comparison of theory and experiment," *Energy & Fuels*, vol. 32, pp. 4300–4307, 2018.
- [49] M. Vereshchak, I. Manakova, A. Shokanov, and S. Sakhiyev, "Mössbauer Studies of Narrow Fractions of Fly Ash Formed after Combustion of Ekibastuz Coal," *Materials*, vol. 14, Article ID 7473, 2021.
- [50] B. Valentim, N. Shreya, B. Paul et al., "Characteristics of ferrospheres in fly ashes derived from Bokaro and Jharia (Jharkhand, India) coals," *International Journal of Coal Geology*, vol. 153, pp. 52–74, 2016.
- [51] V. K. Yadav, G. Gnanamoorthy, M. M. S. Cabral-Pinto et al., "Variations and similarities in structural, chemical, and elemental properties on the ashes derived from the coal due to their combustion in open and controlled manner," *Environmental Science and Pollution Research*, vol. 28, pp. 32609–32625, 2021.
- [52] A. Fauzi, M. F. Nuruddin, A. B. Malkawi, and M. M. A. B. Abdullah, "Study of fly ash characterization as a cementitious material," *Procedia Engineering*, vol. 148, pp. 487–493, 2016.
- [53] W. K. W. Lee and J. S. J. van Deventer, "Structural reorganisation of class F fly ash in alkaline silicate solutions," *Colloids and Surfaces A: Physicochemical and Engineering Aspects*, vol. 211, pp. 49–66, 2002.
- [54] M. Hanesch, "Raman spectroscopy of iron oxides and (oxy) hydroxides at low laser power and possible applications in environmental magnetic studies," *Geophysical Journal International*, vol. 177, pp. 941–948, 2009.
- [55] V. K. Yadav, R. Suriyaprabha, G. K. Inwati et al., "A noble and economical method for the synthesis of low cost zeolites from coal fly ash waste," *Advances in Materials and Processing Technologies*, pp. 1–19, 2021.
- [56] S. Dwivedi, Q. Saquib, A. A. Al-Khedhairi, A.-Y. S. Ali, and J. Musarrat, "Characterization of coal fly ash nanoparticles and induced oxidative DNA damage in human peripheral blood mononuclear cells," *Science of the Total Environment*, vol. 437, pp. 331–338, 2012.
- [57] D. Havlíček, R. Přibíl, and B. Kratochvíl, "Content of quartz and mullite in some selected power-plant fly ash in Czechoslovakia," *Atmospheric Environment*, vol. 23, no. 3, pp. 701–706, 1989.
- [58] N. D. Nugroho, W. Rosita, I. Perdana, I. M. Bendiyasa, F. R. Mufakhir, and W. Astuti, "Iron bearing oxide minerals separation from rare earth elements (REE) rich coal fly ash," *IOP Conference Series: Materials Science and Engineering*, vol. 478, article 012026, 2019.
- [59] P. K. Sahoo, K. Kim, M. A. Powell, and S. M. Equeenuddin, "Recovery of metals and other beneficial products from coal fly ash: a sustainable approach for fly ash management," *International Journal of Coal Science & Technology*, vol. 3, pp. 267–283, 2016.
- [60] M. Y. A. Mollah, S. Promreuk, R. Schennach, D. L. Cocke, and R. Güler, "Cristobalite formation from thermal treatment of Texas lignite fly ash," *Fuel*, vol. 78, pp. 1277–1282, 1999.
- [61] D. Mohan, K. P. Singh, G. Singh, and K. Kumar, "Removal of dyes from wastewater using flyash, a low-cost adsorbent," *Industrial & Engineering Chemistry Research*, vol. 41, pp. 3688–3695, 2002.
- [62] S. Wang, Y. Boyjoo, and A. Choueib, "A comparative study of dye removal using fly ash treated by different methods," *Chemosphere*, vol. 60, pp. 1401–1407, 2005.
- [63] N. Choudhary, V. K. Yadav, K. K. Yadav et al., "Application of green synthesized MMT/Ag nanocomposite for removal of methylene blue from aqueous solution," *Water*, vol. 13, no. 22, p. 3206, 2021.
- [64] R. Lafi, I. Montasser, and A. Hafiane, "Adsorption of Congo red dye from aqueous solutions by prepared activated carbon with oxygen-containing functional groups and its regeneration," *Adsorption Science & Technology*, vol. 37, pp. 160–181, 2019.
- [65] T. H. T. Nguyen, T. T. U. Dao, G. V. Pham et al., "Effect of pH on the adsorption behaviour of Congo red dye on the Mg-Al layered double hydroxide," *IOP Conference Series: Materials Science and Engineering*, vol. 736, article 022077, 2020.